The Astrophysical Journal Letters, 728:L4 (6pp), 2011 February 10 doi:10.1088/2041-8205/728/1/L4

SPITZER IMAGING OF *HERSCHEL*-ATLAS GRAVITATIONALLY LENSED SUBMILLIMETER SOURCES

R. Hopwood[1], J. Wardlow[2], A. Cooray[2], A. A. Khostovan[2], S. Kim[2], M. Negrello[1], E. da Cunha[3], D. Burgarella[4], I. Aretxaga[5], R. Auld[6], M. Baes[7], E. Barton[2], F. Bertoldi[8], D. G. Bonfield[9], R. Blundell[10], S. Buttiglione[11], A. Cava[12,13], D. L. Clements[14], J. Cooke[3,15], H. Dannerbauer[16], A. Dariush[6,17], G. de Zotti[11,18], J. Dunlop[19], L. Dunne[20], S. Dye[6], S. Eales[6], J. Fritz[7], D. Frayer[21], M. A. Gurwell[10], D. H. Hughes[5], E. Ibar[22], R. J. Ivison[22,23], M. J. Jarvis[9], G. Lagache[24,25], L. Leeuw[26,27], S. Maddox[20], M. J. Michałowski[23], A. Omont[28], E. Pascale[6], M. Pohlen[6], E. Rigby[20], G. Rodighiero[29], D. Scott[30], S. Serjeant[1], I. Smail[31], D. J. B. Smith[20], P. Temi[32], M. A. Thompson[9], I. Valtchanov[33], P. van der Werf[23,34], A. Verma[35], and J. D. Vieira[15]

[1] Department of Physics and Astronomy, The Open University, Milton Keynes, MK7 6AA, UK
[2] Department of Physics and Astronomy, University of California, Irvine, CA 92697, USA
[3] Department of Physics, University of Crete, Heraklion, Greece
[4] Laboratoire d'Astrophysique de Marseille, OAMP, CNRS, Aix-Marseille Université, France
[5] Instituto Nacional de Astrofísica, Óptica y Electrónica, Aptdo. Postal 51 y 216, 72000 Puebla, Mexico
[6] School of Physics and Astronomy, Cardiff University, Cardiff, CF24 3AA, UK
[7] Sterrenkundig Observatorium, Universiteit Gent, Krijgslaan 281 S9, B-9000 Gent, Belgium
[8] Argenlander Institute for Astronomy, University of Bonn, Auf dem Hugel 71, 53121 Bonn, Germany
[9] Centre for Astrophysics Research, Science and Technology Research Centre, University of Hertfordshire, Herts AL10 9AB, UK
[10] Harvard-Smithsonian Center for Astrophysics, Cambridge, MA 02138, USA
[11] INAF, Osservatorio Astronomico di Padova, Vicolo Osservatorio 5, I-35122 Padova, Italy
[12] Instituto de Astrofisica de Canarias, C/Va Lactea s/n, E-38200 La Laguna, Spain
[13] Departamento de Astrofisica, Universidad de La Laguna (ULL), E-38205 La Laguna, Tenerife, Spain
[14] Astrophysics Group, Physics Department, Imperial College London, Prince Consort Road, London SW7 2AZ, UK
[15] California Institute of Technology, MS 249-17, 1216 E. California Blvd., Pasadena, CA 91125, USA
[16] Laboratoire AIM Paris Saclay, CEA-CNRS-Université, Irfu/Service d'Astrophysique, CEA Saclay, Orme de Merisiers, 91191 Gif-sur-Yvette Cedex, France
[17] School of Astronomy, Institute for Research in Fundamental Sciences (IPM), PO Box 19395-5746, Tehran, Iran
[18] Scuola Internazionale Superiore di Studi Avanzati, Via Bonomea 265, I-34136 Trieste, Italy
[19] SUPA, Institute for Astronomy, University of Edinburgh, Royal Observatory, Edinburgh, EH9 3HJ, UK
[20] School of Physics and Astronomy, University of Nottingham, University Park, Nottingham NG7 2RD, UK
[21] National Radio Astronomy Observatory P.O. Box 2, Green Bank, WV 24944, USA
[22] UK Astronomy Technology Center, Royal Observatory Edinburgh, Edinburgh, EH9 3HJ, UK
[23] Scottish Universities Physics Alliance, University of Edinburgh, Royal Observatory, Edinburgh, EH9 3HJ, UK
[24] Institut d'Astrophysique Spatiale (IAS), Batiment 121, Universite Paris-Sud 11 91405 Orsay Cedex, France
[25] CNRS (UMR 8617), 91405 Orsay, France
[26] Physics Department, University of Johannesburg, P.O. Box 524, Auckland Park 2006, South Africa
[27] SETI Institute, Mountain View, CA, 94043, USA
[28] Institut d'Astrophysique de Paris, Universitte Pierre et Marie Curie and CNRS, 98 bis boulevard Arago, 75014 Paris, France
[29] Dipartimento di Astronomia, Universita di Padova, Vicolo Osservatorio 2, I-35122 Padova, Italy
[30] Department of Physics and Astronomy, University of British Columbia, Vancouver, BC V6T 1Z1, Canada
[31] Institute for Computational Cosmology, Durham University, South Road, Durham, DH1 3LE, UK
[32] Astrophysics Branch, NASA Ames Research Center, Mail Stop 245-6, Moffett Field, CA 94035, USA
[33] Herschel Science Centre, European Space Agency, P.O. Box 78, 28691 Villanueva da la Cañada, Madrid, Spain
[34] Leiden Observatory, Leiden University, P.O. Box 9513, NL 2300 Leiden, The Netherlands
[35] Oxford Astrophysics, Denys Wilkinson Building, University of Oxford, Keble Road, Oxford, OX1 3RH, UK
Received 2010 November 22; accepted 2010 December 20; published 2011 January 18

ABSTRACT

We present physical properties of two submillimeter selected gravitationally lensed sources, identified in the *Herschel* Astrophysical Terahertz Large Area Survey. These submillimeter galaxies (SMGs) have flux densities >100 mJy at 500 μm, but are not visible in existing optical imaging. We fit light profiles to each component of the lensing systems in *Spitzer* IRAC 3.6 and 4.5 μm data and successfully disentangle the foreground lens from the background source in each case, providing important constraints on the spectral energy distributions (SEDs) of the background SMG at rest-frame optical–near-infrared wavelengths. The SED fits show that these two SMGs have high dust obscuration with $A_V \sim 4$–5 and star formation rates of $\sim 100\,M_\odot\ \mathrm{yr}^{-1}$. They have low gas fractions and low dynamical masses compared with 850 μm selected galaxies.

Key words: galaxies: individual (SDP.81: H-ATLAS J090311.6+003906, SDP.130: H-ATLAS J091305.0-005343) – galaxies: starburst – gravitational lensing: strong

Online-only material: color figures

1. INTRODUCTION

Gravitational lensing is an invaluable astrophysical tool. It can be exploited to study galaxies beyond instrumental blank field sensitivities and to constrain the total mass of galaxy systems, without regard for its dark or luminous nature (see review by Treu 2010). The magnification of distant galaxies through gravitational lensing enables the detailed study of sources that would otherwise be undetectable. In the submillimeter regime, this includes members of the population of intrinsically faint galaxies that comprise a significant fraction of the cosmic far-infrared background.

The *Herschel*[36] (Pilbratt et al. 2010) Astrophysical Large Area Survey (H-ATLAS; Eales et al. 2010) is the largest open-time key project currently being undertaken by *Herschel* and aims to survey 550 deg^2 and detect >300,000 galaxies. A new methodology for selecting gravitational lenses using wide-area submillimeter (sub-mm) surveys (Blain 1996; Perrotta et al. 2002; Negrello et al. 2007) has been tested for the first time during *Herschel*'s science demonstration phase (SDP; Negrello et al. 2010, N10 hereafter). Candidates are selected using a flux cut of 100 mJy at 500 μm, a limit based on the steep number counts slope in the sub-mm (Negrello et al. 2007). Above this flux limit only gravitationally lensed objects and easily identifiable "contaminants" remain, e.g., blazars and local spiral galaxies. Initial results show that this selection method has ~100% efficiency and should deliver a sample of hundreds of new gravitational lenses in planned wide area *Herschel* surveys, probing galaxies with intrinsic fluxes below the *Herschel* confusion limit.

Five lens candidates in the SDP H-ATLAS data (Pascale et al. 2010; Rigby et al. 2010; N10) were confirmed with spectroscopic redshifts obtained via the detection of carbon monoxide (CO) emission lines (Lupu et al. 2010; Frayer et al. 2010) of the background galaxies and optical spectra (Negrello et al. 2010) of the lens galaxies. In this Letter, we study two of these gravitational lenses, H-ATLAS J090311.6+003906 (SDP.81) and H-ATLAS J091305.0-005343 (SDP.130), which are submillimeter galaxy (SMG) at redshifts of $z = 3.04$ and $z = 2.63$ being lensed by ellipticals at $z = 0.30$ and $z = 0.22$, respectively. Submillimeter Array (SMA) imaging reveals the sub-mm morphology, consistent with a lensing event, with multiple peaks distributed around the position of the foreground elliptical galaxy (N10). While no lensed background images were detectable in optical imaging, the spectral energy distribution (SED) models suggest that flux from the background sources should be detectable above ~10 μJy at near-IR wavelengths, from 2 to 5 μm (N10). At these wavelengths, the emission from the foreground lenses, at $z \sim 0.25$, and the background SMGs becomes comparable.

In this Letter, we present *Spitzer*/IRAC imaging, light profile models, photometry, and physical characteristics for SDP.81 and SDP.130 derived from SED fitting. In the next section, we present a summary of the *Spitzer* data, while in Section 3 we discuss modeling of the light profile of the foreground lenses. We perform SED modeling of background SMGs and present results related to the properties of these two sources in Section 4. Throughout the Letter, we assume flat ΛCDM cosmology with $\Omega_M = 0.3$ and $H_0 = 70$ km s^{-1} Mpc^{-1}.

2. *SPITZER* IR AND KECK OPTICAL IMAGING DATA

The IR imaging data are part of *Spitzer* program 548 (PI: A. Cooray), released for analysis on 2010 July 30. For this program, Infrared Array Camera (IRAC; Fazio et al. 2004) images of SDP.81 and SDP.130 were taken at 3.6 μm (Channel 1) and 4.5 μm (Channel 2). Both lensing systems were imaged with a 36-position dither pattern and an exposure time of 30 s for each frame to achieve an effective total exposure time of 1080 s. The rms depth reached is 0.3 and 0.4 μJy in Channels 1 and 2, respectively.

[36] *Herschel* is an ESA space observatory with science instruments provided by European-led Principal Investigator consortia and with important participation from NASA.

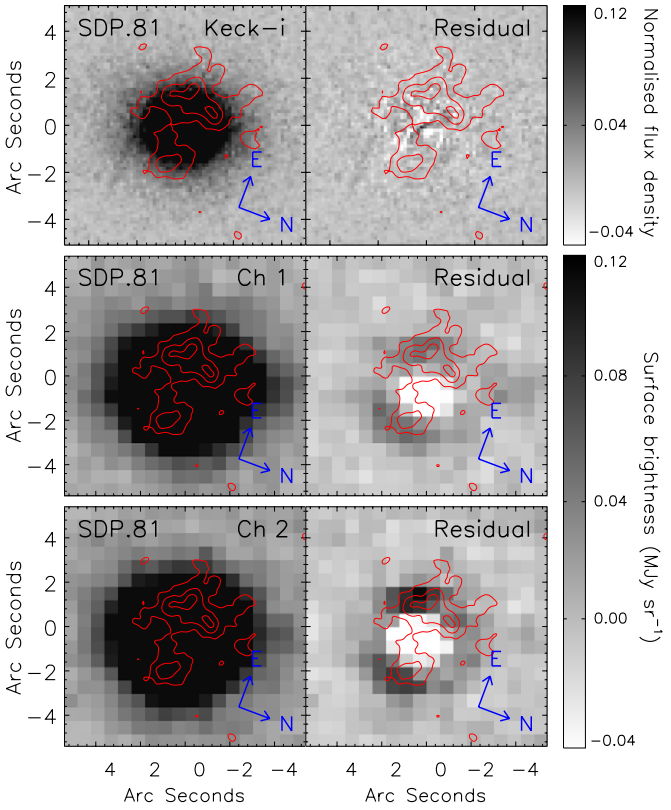

Figure 1. Keck *i*-band (top row), IRAC Channel 1 (middle row), and Channel 2 (bottom row) postage stamp images for SDP.81. The corresponding residual (right column) is presented after subtraction of single de Vaucouleurs profiles modeled on the Keck *i*-band data. The Keck residuals show no signs of structure associable with the overlaid 880 μm SMA signal-to-noise ratio (S/N) contours. For the IRAC residual there is structure that can be associated with the SMA contours, which suggests this is lensed structure of the respective background galaxy. The SMA contours are overlaid in steps of 3σ, 8σ, 13σ, etc. SMA peaks with S/N > 8 (four for ID81 and two for ID130) have a maximum rms on the position of a point source of 0.″1. All postage stamps are plotted with the same pixel intensity scaling after normalizing the Keck *i*-band data to the dynamic pixel value range of the IRAC data.

(A color version of this figure is available in the online journal.)

Corrected basic calibrated data pre-processed by the *Spitzer* Science Center (SSC), using the standard pipeline version S18.18.0, were spatially aligned, resampled, and combined into a mosaic image using version 18.3.1 of the SSC's MOPEX software suite (Makovoz & Marleau 2005). The IRAC mosaics have a resampled pixel size of 0.″6 and angular resolution of 2″–2.″5. For the work presented here, we also use the IRAC point-spread function (PSF; version 2010 April) file as provided by the SSC[37].

We also make use of optical images of SDP.81 and SDP.130 that were acquired on 2010 March 10 using the dual-arm Low Resolution Imaging Spectrometer (LRIS; Oke et al. 1995; McCarthy et al. 1998) on the Keck I telescope and reported in N10 (see Figures 1 and 2). Each target received simultaneous 3 × 110 s integrations with the *g*-filter and 3 × 60 s integrations with the *i*-filter using the blue and red arms of LRIS, respectively. A 20″ dither pattern was employed to generate on-sky flat-field frames. We performed photometric calibration using 1 s *g*- and *i*-band observations of bright stars in each field. The data were reduced using IDL routines and combined and analyzed using

[37] http://ssc.spitzer.caltech.edu/irac/calibrationfiles/psfprf/

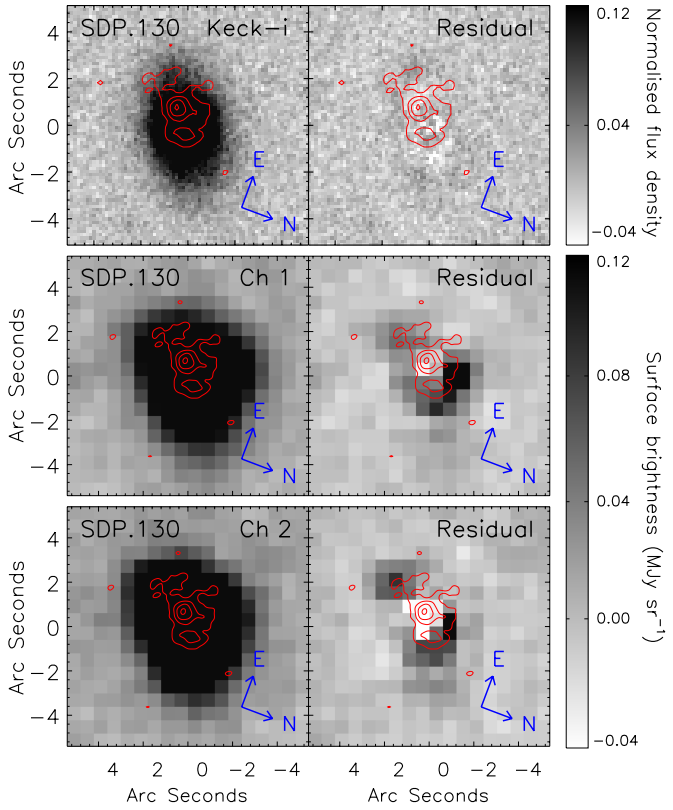

Figure 2. Keck *i*-band (top row), IRAC Channel 1 (middle row) and Channel 2 (bottom row) postage stamp images for SDP.130. The corresponding residuals are presented after subtraction of single de Vaucouleurs profiles modeled on the Keck *i*-band data. Although the Keck residuals show no signs of significant structure, the subtracted IRAC data have residual structure that can be associated with the SMA contours, which suggests lensed structure of the respective background galaxy is present. The SMA contours are presented as in Figure 1. All postage stamps are plotted with the same pixel intensity scaling after normalizing the Keck *i*-band data to the dynamic pixel value range of the IRAC data.

(A color version of this figure is available in the online journal.)

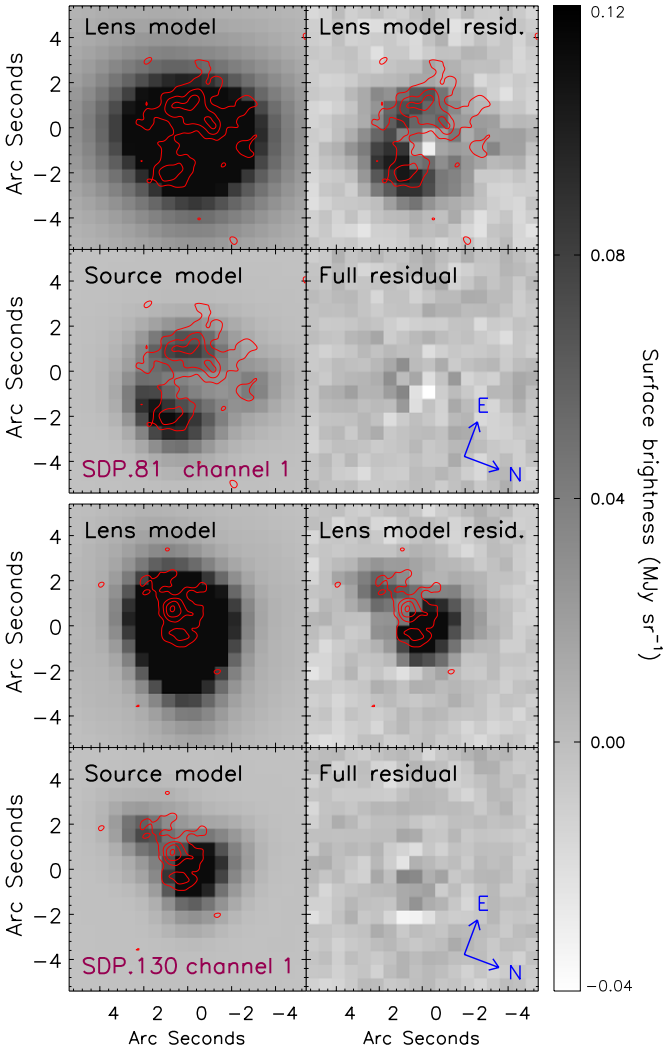

Figure 3. Multi-component light profile models for SDP.81 (top) and SDP.130 (bottom), for the IRAC Channel 1 data. Shown are the unsubtracted data, the lens model (a single Sérsic profile for SDP.81 and a Sérsic plus exponential disk profile for SDP.130), the residual after subtraction of the lens model profile only and the total model residual (full residual). The SMA contours are presented as in Figure 1. All data are plotted with the same pixel intensity scaling.

(A color version of this figure is available in the online journal.)

standard IRAF tasks; the seeing FWHM of the final science exposures is ∼0.″8.

3. MODELING THE LENSES

To construct models of the light profiles for each lensing system we use GALFIT (Peng et al. 2002), which allows multiple profiles per object and performs a simultaneous nonlinear minimization. Prior to fitting profiles to SDP.81 and SDP.130 in the IRAC data, de Vaucouleurs profile (de Vaucouleurs 1948) models are constructed for the Keck *i*-band imaging, to take advantage of the comparatively higher resolution of these images, and the presence of only one component per system, i.e., the lens galaxy.

To look for any potentially lensed structure in the IRAC data, the Keck models are used to fit the IRAC Channels 1 and 2 data, keeping the effective radius and ellipticity fixed, and using the appropriate IRAC PSF[37]. On subtraction of the results, and in comparison to the model subtracted Keck data and SMA contours, the IRAC band residuals strongly suggest that a more complex structure, associated with the background SMG, is present for both SDP.81 and SDP.130 (see Figures 1 and 2).

We verify that these residuals are significant, and not an artifact of imperfections in the IRAC PSF, by comparing them with residuals derived for three (non-lensing) elliptical-like galaxies in the same field, after fitting them with single Sérsic profiles. For both the lensing systems and the comparison ellipticals aperture flux ratios were determined for the residual image and the corresponding unsubtracted data. To consider only positive structure, pixel values $>2\sigma$ below the local background were replaced with the median local sky value. The SMG residuals were found to have flux ratios ∼3–5 greater than those for the random elliptical galaxies.

In order to more precisely disentangle the lens and background components we represent the flux from the lensed SMGs with Sérsic profiles. Peaks were identified in the IRAC single profile fit residual images, by fitting Gaussian profiles. We add three profiles for SDP.81 and two for SDP130, which all correspond to significant sub-mm contour peaks in the SMA data, within 0.″8. N10 modeled the Keck *i* band with a Sérsic profile plus an exponential disk, as this combination gave a marginally improved χ^2 over single profile models, and found that the exponential component significantly contributes to the total profile for SDP.130. Therefore, a Sérsic plus exponential disk profile is adopted for the SDP.130 lens and a single Sérsic

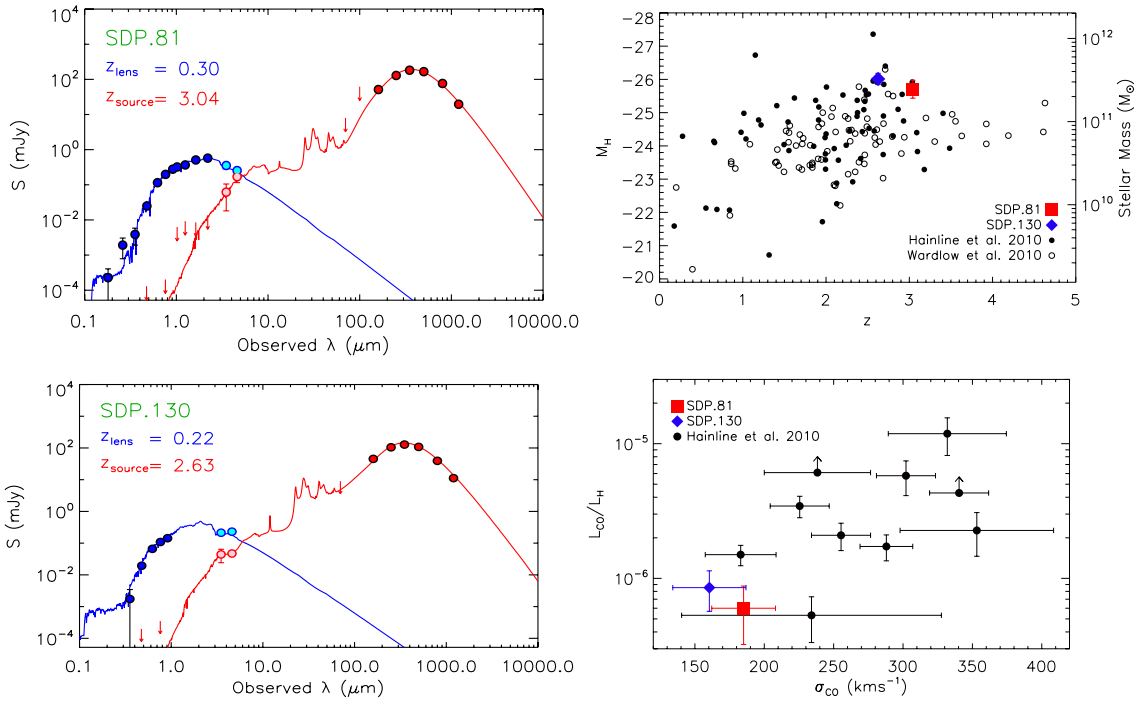

Figure 4. Left: photometry and best-fit SEDs for the foreground elliptical (blue) and background SMG (red) for SDP.81 and SDP.130. The photometric points and upper limits are taken from Negrello et al. (2010), with updated PACS flux densities at 160 μm and upper limits at 70 μm. Photometry from the best-fitting light profiles to the IRAC data are added for the foreground lens galaxies (turquoise points) and for the background SMG (pink points). The SEDs are fitted using the models of da Cunha et al. (2008). We find that high levels of visual extinction of the SMGs are required ($A_V > 4$) to be consistent with the optical–near-IR data. Top right: a plot of (magnification corrected) rest-frame absolute H-band (M_H) magnitude against redshift for SDP.81 and SDP.130, showing the approximate correspondence of M_H with stellar mass. For comparison, we also show 850 and 870 μm selected galaxies (Hainline et al. 2010; Wardlow et al. 2010). The two lensed H-ATLAS sources are brighter than ∼95% of the comparison sample, and correspondingly, are likely to be amongst the most massive. Error bars are omitted from the comparison sample for clarity. Bottom right: ratio of CO and H-band luminosity against CO line velocity for the H-ATLAS lensed galaxies and 850 μm selected SMGs. L_{CO}/L_H is independent of the lensing model (to the first order; see discussion in the text) and represents the gas-to-stellar mass ratio. σ_{CO} is indicative of dynamical mass, although it also depends on the inclination angle and size of the CO emitting region, which increases the observed scatter. SDP.81 and SDP.130 have small dynamical masses and small gas fractions, relative to the comparison sample.

(A color version of this figure is available in the online journal.)

profile for the SDP.81 lens. To produce the final models for the lens and background galaxies, we refit the profile representing the lens galaxy and the additional Sérsic profiles simultaneously for each system with GALFIT. These final model fits for the background component of SDP.81 show a partial "Einstein ring"-like morphological structure for the lensed source (Figure 3). For SDP.130, the lensed component is more compact and in close proximity to the lens profile. The resulting best-fit profiles for the background galaxies agree well with the SMA contours, and the combined models subtract cleanly, suggesting successful lens/source decoupling.

4. SPECTRAL ENERGY DISTRIBUTION OF THE LENSED SMGs

The GALFIT-integrated magnitudes for each component of the final SDP.81 and SDP.130 models were converted to flux density to extend the existing multi-waveband photometry (see Table 1 and N10, and references therein) into the near-IR. We assign 1σ errors to the photometry obtained from the final GALFIT model profiles, using the magnitude distributions for all the GALFIT trials that converged. PACS re-imaging of the lensed H-ATLAS sources provides new photometry at 160 μm and upper limits at 70 μm (I. Valtchanov et al. 2011, in preparation; Ibar et al. 2010). For the goal of deriving physical properties, the IRAC photometry adds particularly important constraints to the SMG SEDs, which previously consisted of just upper limits at wavelengths below 250 μm for SDP.130 and 160 μm for SDP.81.

The SEDs of the SMGs are fitted using the models of da Cunha et al. (2008), calibrated to reproduce the ultraviolet-to-infrared SEDs of local, purely star-forming Ultra Luminous Infrared Galaxies (ULIRGs; $10^{12} \leqslant L_{IR}/L_{\odot} < 10^{13}$; da Cunha et al. 2010). The SED models assume a Chabrier (2003) initial mass function (IMF) that is cutoff below 0.1 and above 100 $M_{\odot}$; using a Salpeter IMF instead gives stellar masses that are a factor of ∼1.5 larger. We find that a significant attenuation by dust ($A_V \sim 4$–5) is required to be consistent with the IRAC photometry and optical/near-IR upper limits (Figure 4), which is consistent with other ULIRGs and SMGs (e.g., Geach et al. 2007; Hainline et al. 2010; Michałowski et al. 2010; Wardlow et al. 2010).

Using the Chabrier (2003) IMF, with parameters derived from the SED fits, we find that SDP.81 and SDP.130 have stellar masses ($M_{\star}$) of $(2.5 \pm 1.7) \times 10^{11}\ M_{\odot}$ and $(4.5 \pm 2.5) \times 10^{11}\ M_{\odot}$, respectively (see Table 1). However, we note that there is an additional systematic error of up to a factor of 10, due to uncertainty in the appropriate mass-to-light ratio (see Wardlow et al. 2010 for a discussion) and magnification factors, as well as a lack of observations at optical/near-IR wavelengths. J and Ks photometric data on these galaxies with VLT/HAWK-I observations (A. Verma et al. 2011, in preparation) could potentially improve the estimates of extinction and stellar mass.

Rest-frame absolute H-band magnitudes (M_H) provide a guide to galaxy stellar masses that is not complicated by the details

Table 1
Parameters of the Foreground Lens and Background SMG for SDP.81 and SDP.130

Parameters	SDP.81	SDP.130
Foreground lens		
R.A.	$09^h03^m11\overset{s}{.}6$	$09^h13^m05\overset{s}{.}0$
Decl.	$00^d39^m06^s$	$-00^d53^m43^s$
Redshift[a]	0.299	0.220
SDSS u (μJy)	3.9 ± 2.0	1.7 ± 1.7
SDSS g (μJy)	24.9 ± 1.1	19.4 ± 0.7
SDSS r (μJy)	115 ± 2	66.1 ± 1.2
SDSS i (μJy)	198 ± 4	109 ± 2
SDSS z (μJy)	278 ± 8	143 ± 7
UKIDSS Y (μJy)	320 ± 20	...
UKIDSS J (μJy)	370 ± 20	...
UKIDSS H (μJy)	510 ± 50	...
UKIDSS K (μJy)	570 ± 70	...
Spitzer 3.6 μm (mJy)	0.35 ± 0.04	0.213 ± 0.03
Spitzer 4.5 μm (mJy)	0.22 ± 0.04	0.230 ± 0.01
Background SMG: observed quantities		
Redshift[a]	3.042	2.625
Magnification[a]	25 ± 7	6 ± 1
Keck/LRIS g (μJy)	< 0.13	< 0.20
Keck/LRIS i (μJy)	< 0.20	< 0.35
UKIDSS Y (μJy)	< 6.27	...
UKIDSS J (μJy)	< 9.23	...
UKIDSS H (μJy)	< 8.52	...
UKIDSS K (μJy)	< 13.5	...
Spitzer 3.6 μm (mJy)	0.062 ± 0.04	0.044 ± 0.01
Spitzer 4.5 μm (mJy)	0.126 ± 0.05	0.047 ± 0.01
PACS 70 μm (mJy)[b]	< 8.0	< 9.0
PACS 100 μm (mJy)	< 62	...
PACS 160 μm (mJy)[b]	51 ± 5	45 ± 8
SPIRE 250 μm (mJy)	130 ± 20	105 ± 17
SPIRE 350 μm (mJy)	180 ± 30	128 ± 20
SPIRE 500 μm (mJy)	170 ± 30	108 ± 18
SMA 880 μm (mJy)	76 ± 4	39 ± 2
IRAM 1200 μm (mJy)	19.6 ± 0.9	11.2 ± 1.2
Background SMG: derived quantities		
L_{IR} (10^{12} $L_\odot$)[c]	2.0 ± 0.6	5.6 ± 1.2
A_V	4.4 ± 0.6	5.0 ± 0.5
M_H	-25.7 ± 0.3	-26.01 ± 0.17
SFR ($M_\odot$ yr^{-1})	74 ± 30	150 ± 50
$M(H_2)$ (10^{10} $M_\odot$)[d]	1.4	2.7
$M_\star$ (10^{11} $M_\odot$)[e]	2.5 ± 1.7	4.5 ± 2.5
M_{dust} (10^8 $M_\odot$)[f]	3.4 ± 1.0	11 ± 2
μ[g]	0.05 ± 0.01	0.08 ± 0.01

Notes. The optical and sub-mm flux densities and 3σ upper limits are taken from N10, unless otherwise noted. Derived quantities are corrected for magnification and the errors quoted account for the tabulated uncertainty in the magnification.
[a] Spectroscopic redshifts (N10).
[b] From PACS re-imaging data (I. Valtchanov et al. 2011, in preparation; Ibar et al. 2010).
[c] 2 to 1000 μm luminosity based on the best-fit SED.
[d] Frayer et al. 2010, uncertainty is at least a factor of $\sim$2.
[e] There is an additional systematic uncertainty up to a factor of $\sim$10 (see the text).
[f] Calculated with a dust mass absorption coefficient approximated as $\kappa_\lambda \propto \lambda^\beta$ with $\beta = 1.5$ for warm dust and $\beta = 2$ for cold dust, and a normalization of 0.77 g^{-1} cm^2 at 850 μm. There is an additional systematic uncertainty of at least a factor of $\sim$2.
[g] Gas fraction, $\mu = M(H_2)/[M_\star + M(H_2)]$, uncertainty is a factor of 2–3.

of the assumed star formation history and is straightforward to compare to other similarly selected samples. In the top panel of Figure 4, we plot M_H against redshift for SDP.81 and SDP.130 compared to 850 and 870 μm selected SMGs (Hainline et al. 2010; Wardlow et al. 2010). The H-ATLAS-lensed galaxies are brighter than the majority of the 850–870 μm selected SMGs, thus if there is no active galactic nucleus contribution to their H-band luminosities they are likely to be amongst the most massive.

We next consider the CO(1–0)-to-H-band luminosity ratio (L_{CO}/L_H), a representation of the gas-to-stellar mass fraction that is mostly independent of the lensing model. However, the IRAC data trace stellar emission, which may originate from a spatially different region of the SMG to the far-infrared emission. As such there may be variation in the lensing amplifications across the source plane, potentially leading to a small effect on L_{CO}/L_H. The bottom panel of Figure 4 shows L_{CO}/L_H against the CO line width (σ_{CO}) for the two H-ATLAS lensed galaxies, compared to 850 μm selected SMGs (Hainline et al. 2010). σ_{CO} is independent of L_{CO}/L_H and is indicative of the dynamical mass of the system, although some scatter is introduced due to the dependence on the inclination angle and the size of the CO emitting region. Published CO luminosities of the 850 μm selected sample (Greve et al. 2005; Coppin et al. 2008; Frayer et al. 2008; Tacconi et al. 2008; Bothwell et al. 2010) are converted to the equivalent CO(1–0) values using $L_{CO(3-2)}/L_{CO(1-0)} = 0.6$ and $L_{CO(4-3)}/L_{CO(1-0)} = 0.6$ (Ivison et al. 2010). Galaxies with poorly defined σ_{CO} are excluded. The H-ATLAS-lensed galaxies have low L_{CO}/L_H (representative of gas fraction) and low σ_{CO} (representative of dynamical mass) compared to 850 μm selected galaxies (Figure 4). There may also be a weak inverse trend between L_{CO}/L_H and σ_{CO} for all the SMGs, although a larger sample is required for confirmation.

Summary. We have studied the background SMGs of two sub-mm bright gravitational lenses, identified in the H-ATLAS SDP data. The intrinsic sub-mm flux densities of these SMG are below the *Herschel* confusion noise and, therefore, undetectable without the fortuitous lensing by foreground ellipticals. The full 550 deg^2 survey area of H-ATLAS will recover a sample of >200 lensed SMGs, and *Spitzer* follow-up observations will enable us to study the physical properties of SMGs over a wide range of redshift and far-IR luminosities. Studies such as this are necessary to further understand the nature of sources that contribute to the bulk of the cosmic far-infrared background.

Herschel-ATLAS is a project with *Herschel*, which is an ESA space observatory with science instruments provided by European-led Principal Investigator consortia and with important participation from NASA. The H-ATLAS Web site is http://www.h-atlas.org/ We thank the Science and Technology Facilities Council, grant D/002400/1 and studentship/SF/F005288/1. This work is based in part on observations made with the *Spitzer* Space Telescope, which is operated by the Jet Propulsion Laboratory, California Institute of Technology under a contract with NASA. Support for this work was provided by NASA through an award issued by JPL/Caltech. US participants in H-ATLAS also acknowledge support from NASA *Herschel* Science Center through a contract from JPL/Caltech. I.A. and D.H.H. are partially funded by CONACyT grants 50786 and 60878.

REFERENCES

Blain, A. W. 1996, MNRAS, 283, 1340
Bothwell, M. S., et al. 2010, MNRAS, 405, 219
Chabrier, G. 2003, PASP, 115, 763
Coppin, K., et al. 2008, MNRAS, 389, 45

da Cunha, E., Charlot, S., & Elbaz, D. 2008, MNRAS, 388, 1595
da Cunha, E., Charmandaris, V., Díaz-Santos, T., Armus, L., Marshall, J. A., & Elbaz, D. 2010, A&A, 523, A78
de Vaucouleurs, G. 1948, Ann. Astrophys., 11, 247
Eales, S., et al. 2010, PASP, 122, 499
Fazio, G. G., et al. 2004, ApJS, 154, 10
Frayer, D. T., et al. 2008, ApJ, 680, L21
Frayer, D., et al. 2010, ApJ, 726, L22
Geach, J. E., Smail, I., Chapman, S. C., Alexander, D. M., Blain, A. W., Stott, J. P., & Ivison, R. J. 2007, ApJ, 655, L9
Greve, T. R., et al. 2005, MNRAS, 259, 1165
Hainline, L. J., Blain, A. W., Smail, I., Alexander, D. M., Armus, L., Chapman, S. C., & Ivison, R. J. 2010, MNRAS, submitted (arXiv:1006.0238)
Ibar, E., et al. 2010, MNRAS, 409, 38
Ivison, R. J., Papadopoulos, P. P., Smail, I., Greve, T. R., Thomson, A. P., Xilouris, E. M., & Chapman, S. C. 2010, MNRAS, in press (arXiv: 1009.0749)
Lupu, R., et al. 2010, ApJ, submitted (arXiv:1009.5983)
Makovoz, D., & Marleau, F. R. 2005, PASP, 117, 1113
McCarthy, J. K., et al. 1998, Proc. SPIE, 3355, 81
Michałowski, M. J., Hjorth, J., & Watson, D. 2010, A&A, 514, A67
Negrello, M., Perrotta, F., González-Nuevo, J., Silva, L., de Zotti, G., Granato, G. L., Baccigalupi, C., & Danese, L. 2007, MNRAS, 377, 1557
Negrello, M., et al. 2010, Science, 330, 800
Oke, J. B., et al. 1995, PASP, 107, 375
Pascale, E., et al. 2010, MNRAS, submitted (arXiv:1010.5782)
Peng, C. Y., Ho, L. C., Impey, C. D., & Rix, H.-W. 2002, AJ, 124, 266
Perrotta, F., Baccigalupi, C., Bartelmann, M., De Zotti, G., & Granato, G. L. 2002, MNRAS, 329, 445
Pilbratt, G. L., et al. 2010, A&A, 518, L1
Rigby, E. E., et al. 2010, MNRAS, submitted (arXiv:1010.5787)
Tacconi, L. J., et al. 2008, ApJ, 680, 246
Treu, T. 2010, ARA&A, 48, 87
Wardlow, J. L., et al. 2010, MNRAS, submitted (arXiv:1006.2137)